Journal of Computational Physics **158,** 116–135 (2000)
doi:10.1006/jcph.1999.6410, available online at http://www.idealibrary.com on IDEAL®

Application of the Difference Gaussian Rules to Solution of Hyperbolic Problems

Sergey Asvadurov,* Vladimir Druskin,* and Leonid Knizhnerman†

*Schlumberger-Doll Research, Old Quarry Road, Ridgefield, Connecticut 06877-4108; †Central Geophysical Expedition, Narodnogo Opolcheniya St., 40-3, Moscow 123298, Russia
E-mail: asvadurov@slb.com, druskin@slb.com, mmd@cge.ru

Received May 12, 1999

Two of the authors earlier suggested a method of calculating special grid steps for three point finite-difference schemes which yielded exponential superconvergence of the Neumann-to-Dirichlet map. We apply this approach to solve the two-dimensional time-domain wave problem and the 2.5-D elasticity system in cylindrical coordinates. Our numerical experiments exhibit exponential convergence at prescribed points, with the cost per grid node close to that of the standard second order finite-difference scheme. The scheme demonstrates high accuracy with slightly more than two grid points per wavelength. The reduction of the grid size by one order compared to the standard scheme with the equidistant grids is observed.

Key Words: finite differences; optimal grids; exponential convergence; hyperbolic problems; linear elasticity; wave propagation.

CONTENTS

1. INTRODUCTION

The simplest and most common discretization of second derivatives in elliptic operators is the three-point stencil. Applied to the two- or three-dimensional Laplace operators, it yields five- or seven-point schemes, respectively, with second order convergence. Such sparse schemes are convenient for the approximation of the spatial part in hyperbolic equations within the framework of finite difference time domain (FDTD) methods, because their

0021-9991/00 $35.00

computational cost is directly proportional to the stencil's size. However, the second order convergence schemes for wave problems suffer from high numerical dispersion, and they typically require more than sixteen points per wavelength to obtain physically meaningful results. It is well known that an optimal discretization scheme can represent a signal with only two grid points per period (the Nyquist limit). Conventionally, close-to-optimal discretizations with exponential convergence can be obtained by more computationally expensive spectral and pseudospectral methods with full stencil requiring FFT for time-stepping [1].

A standard three-point finite-difference approximation of a second order operator ODE on a nonequidistant grid was considered in [2], and it was shown that the optimization of the grid with respect to the error of the boundary impedance (the Neuman-to-Dirichlet map) is equivalent to the optimization of a deviation of a rational function from the true impedance on a given spectral interval. The grid optimization can be viewed as an implementation of the concept of the Gaussian quadrature rules to the three-point finite differences. A Gaussian k-point quadrature is chosen to be exact for $2k$ trial functions, and the optimal grid with k nodes is chosen in such a way that the $2k$ moments of the finite-difference impedance are exact. An approximate solution of this optimization problem was given in [3] using the Padé–Chebyshev approximant. This solution yielded exponential convergence of the impedance, i.e., the standard second order scheme with the three-point stencil exhibited spectral superconvergence at a prescribed boundary. In the follow-up paper [4] the suggested scheme was applied to the two-dimensional Helmholtz equation with piecewise-constant coefficients in a framework similar to that of the multidomain spectral method with tensor-product grids. The resulting scheme coincides with the standard five-point finite-difference scheme in the interior of the homogeneous subdomains and has up to eight additional points at the interfaces; however, it exhibits the spectral convergence at subdomain corners. We should stress that globally the obtained scheme still converges similarly to the standard discretization with a five-point stencil, i.e., behaves as a second-order scheme with respect to the maximal grid step. The new approach, though, is ideally suited for geophysical applications where the solution is needed only at a few receiver points.

Here we apply this scheme within an FDTD framework for the solution of a scalar two-dimensional wave equation and a 2.5-dimensional elasticity system arising from acoustic logging in the semisoft layered formation with the fluid filled borehole. We used the first order system approach which simplifies the implementation of the optimal grids compared to the second order PDE approach exploited in [3, 4]. For simplicity the grid is optimized only along one coordinate axis. We observe that the optimal grid requires two to three grid points per minimal wavelength in the model to obtain about two percent accuracy at the receivers. This results in one order reduction of the grid size compared to the standard equidistant FDTD with the same error, while the computational cost per grid node is approximately the same for both methods.

2. SPECTRALLY OPTIMAL FINITE-DIFFERENCE SCHEMES ON A HOMOGENEITY INTERVAL

Consider a 1-D wave equation on $[0, L] \times [0, T]$, written as a first order system

$$\frac{d\hat{u}}{dt} = \frac{d\hat{v}}{dx}, \qquad \frac{d\hat{v}}{dt} = \frac{d\hat{u}}{dx}, \tag{2.1}$$

with zero initial and some nontrivial boundary conditions. Using Fourier transformation $u = \int \hat{u} e^{-i\omega t}\, dt$, $v = \int \hat{v} e^{-i\omega t}\, dt$, we reduce (2.1) to the first order ODE system

$$\sqrt{\lambda} u = \frac{dv}{dx}, \qquad \sqrt{\lambda} v = \frac{du}{dx}, \tag{2.2}$$

where $\lambda = -\omega^2$. Throughout this paper we assume that u and v vanish for $\omega > \omega_{\max}$, i.e., we are looking for an approximation to the solution of (2.2) on the spectral interval $[\lambda_1, \lambda_2]$, where $\lambda_1 = -\omega_{\max}^2$ and $\lambda_2 = 0$.

First we consider a mixed two-point problem on a segment $[0, L]$, $L > 0$, and consider (2.2) with the boundary conditions

$$v(0) = -1/\sqrt{\lambda}, \qquad u(L) = 0. \tag{2.3}$$

We define the impedance function as $u(0) = f(\lambda)$, i.e.,

$$u(0) = f(\lambda) = \frac{1 - e^{-2L\sqrt{\lambda}}}{\sqrt{\lambda}(1 + e^{-2L\sqrt{\lambda}})} = \frac{2}{L} \sum_{i=1}^{\infty} \frac{1}{\lambda - \xi_i}, \tag{2.4}$$

where $\xi_i = -[\frac{\pi(i-1/2)}{L}]^2$ are the eigenvalues of problem (2.2) with homogeneous boundary conditions. Problem (2.2)–(2.3) is well-posed for any complex λ excluding the resonances ξ_i.

We now approximate (2.2)–(2.3) by a two-point finite-difference scheme. The potential FD solution u is defined at "potential" nodes x_i, $i = 1, \ldots, k+1$, $x_1 = 0$, $x_{i+1} > x_i$; the "derivatives" v are defined at nodes $\hat{x}_i$, $i = 0, \ldots, k$, $\hat{x}_0 = 0$. We denote $h_i = x_{i+1} - x_i$, $\hat{h}_i = \hat{x}_i - \hat{x}_{i-1}$, and solve the FD problem

$$\begin{aligned} \sqrt{\lambda} u_i &= \frac{v_i - v_{i-1}}{\hat{h}_i}, \qquad i = 1, \ldots, k, \; u_{k+1} = 0, \\ \sqrt{\lambda} v_i &= \frac{u_{i+1} - u_i}{h_i}, \qquad i = 1, \ldots, k, \; v_0 = -1/\sqrt{\lambda}. \end{aligned} \tag{2.5}$$

The crucial fact is that $u_1 = f_k(\lambda)$, where the discrete impedance function f_k is a rational function of λ depending on $h_i, \hat{h}_i$ as parameters.

We would like to optimize the location of gridpoints, i.e., of parameters $h_i, \hat{h}_i$, to minimize the error $|f - f_k|$ on a given spectral interval $[\lambda_1, \lambda_2]$. We found that standard methods of constrained optimization fail to provide a reliable answer for $k \geq 5$. We therefore developed an algorithm to compute the grid steps that give almost optimal error. This algorithm can be roughly divided into two steps. In Step 1 we calculate a rational approximation $f_k(\lambda)$ to the impedance function $f(\lambda)$ given by (2.4). This approximation is obtained by the Padé–Chebyshev method and is close to optimal for a given interval of λ. In Step 2 we calculate the parameters $h_i, \hat{h}_i$ that produce a rational function obtained in Step 1.

For consistency with previous publications, we temporarily rewrite the FD scheme (2.5) as a second order system,

$$\lambda u_i - \frac{1}{\hat{h}_i}\left(\frac{u_{i+1} - u_i}{h_i} - \frac{u_i - u_{i-1}}{h_{i-1}}\right) = 0, \qquad i = 2, \ldots, k, \tag{2.6a}$$

$$\lambda u_1 - \frac{1}{\hat{h}_1}\left(\frac{u_2 - u_1}{h_1}\right) = \frac{1}{\hat{h}_1}, \qquad u_{k+1} = 0. \tag{2.6b}$$

The above scheme can be written in the matrix form as

$$\lambda \mathbf{u} - S\mathbf{u} = \hat{h}_1^{-1}\mathbf{e}_1, \qquad \mathbf{u} = (u_1, \ldots, u_k)^T. \tag{2.7}$$

2.1. Rational approximation. To make the operator in (2.7) symmetric, we multiply Eq. (2.6a) by $\hat{h}_i^{1/2}$ and set $w_i = \hat{h}_i^{1/2} u_i$, which yields

$$\lambda \mathbf{w} - H\mathbf{w} = \hat{h}_1^{-1/2}\mathbf{e}_1. \tag{2.8}$$

Here

$$H = H^T = B^{1/2} S B^{-1/2} = \begin{pmatrix} \alpha_1 & \beta_1 & \ldots & 0 \\ \beta_1 & \alpha_2 & \beta_2 & \\ \vdots & & \ddots & \vdots \\ 0 & \ldots & \beta_{k-1} & \alpha_k \end{pmatrix}, \tag{2.9}$$

with $B = \operatorname{diag}\{\hat{h}_i\}$ and

$$\begin{gathered} \alpha_1 = -(\hat{h}_1 h_1)^{-1}, \qquad \beta_1 = (h_1 \sqrt{\hat{h}_1 \hat{h}_2})^{-1}, \\ \beta_i = (h_i \sqrt{\hat{h}_i \hat{h}_{i+1}})^{-1}, \qquad \alpha_i = -\hat{h}_i^{-1}\left(\frac{1}{h_i} + \frac{1}{h_{i-1}}\right), \qquad i = 2, \ldots, k. \end{gathered} \tag{2.10}$$

Denote the eigenvectors of H by $\mathbf{s}_i$ and the corresponding eigenvalues by θ_i. Using eigendecomposition, we can write $H = LDL^T$, where $D = \operatorname{diag}\{\theta_i\}$ and L is the orthogonal matrix consisting of the eigenvectors, $L = [\mathbf{s}_1 \cdots \mathbf{s}_k]$. Multiplying (2.8) by L^T on the left and solving for $\mathbf{w}$, we get $\mathbf{w} = \hat{h}_1^{-1/2} L(\lambda \mathbb{I} - D)^{-1} L^T \mathbf{e}_1$, or

$$u_1 = f_k(\lambda) = \hat{h}_1^{-1} \mathbf{e}_1^T L(\lambda \mathbb{I} - D)^{-1} L^T \mathbf{e}_1, \tag{2.11}$$

where $\mathbb{I}$ is the identity matrix. Finally, we get

$$f_k(\lambda) = \sum_{i=1}^{k} \frac{y_i}{\lambda - \theta_i}, \tag{2.12}$$

where $y_i = s_i^2 / \hat{h}_1$ and s_i are the first components of vectors $\mathbf{s}_i$.

We seek a rational function f_k that approximates f given by (2.4) on an interval $[\lambda_1, \lambda_2]$. Ideally we would like to obtain the optimal approximation from minimization of $\max_{[\lambda_1, \lambda_2]} |f(\lambda) - f_k(\lambda)|$, but, as was mentioned earlier, we found it impossible with the help of standard optimization algorithms. Another option is to use Padé approximation, which matches the derivatives of $f(\lambda)$ at some point λ_0 on the interval in question. It can be shown that, since f is a Stieltjes function, Padé approximations will converge exponentially. However, the approximation error grows rapidly away from λ_0. We therefore use Padé–Chebyshev approximations which have better properties on an interval.

The Padé–Chebyshev approximant f_k is defined by the condition

$$\int_{\lambda_1}^{\lambda_2} \lambda^l [f(\lambda) - f_k(\lambda)] \rho(\lambda)\, d\lambda = 0, \tag{2.13}$$

where $\rho(\lambda) = \{1 - [(2\lambda - (\lambda_2 + \lambda_1))/(\lambda_2 - \lambda_1)]^2\}^{-1/2}$ is the Chebyshev spectral weight adjusted to $[\lambda_1, \lambda_2]$ and $l = 0, \ldots, l_{\max} - 1$ with $l_{\max}$ the number of optimization parameters.

The spectral interval $[\lambda_1, \lambda_2]$ can contain some resonances ξ_i of $f(\lambda)$. Let n, $0 \le n \le k$, be the number of such resonances, and prescribe the first n terms of $f_k(\lambda)$ to be the same as the ones of (2.4), i.e., look for $f_k(\lambda)$ of the form

$$f_k(\lambda) = \frac{2}{L} \sum_{i=1}^{n} \frac{1}{\lambda - \xi_i} + \sum_{i=n+1}^{k} \frac{y_i}{\lambda - \theta_i}. \tag{2.14}$$

We clearly have now only $l_{\max} = 2k - 2n$ parameters of optimization, and thus the problem of approximation is defined as follows:

Step 1. Find y_i, θ_i, $i = n+1, \ldots, k$, such that

$$\int_{\lambda_1}^{\lambda_2} \lambda^l \left[\sum_{i=n+1}^{k} \frac{y_i}{\lambda - \theta_i} - \frac{2}{L} \sum_{i=n+1}^{\infty} \frac{1}{\lambda - \xi_i} \right] \rho(\lambda)\, d\lambda = 0, \qquad l = 0, \ldots, 2k-2n-1. \tag{2.15}$$

For $i = 1, \ldots, n$ set $y_i = 2/L$, $\theta_i = \xi_i$.

The details of calculation of y_i, θ_i are given in [3] for $f(\lambda) = \lambda^{-1/2}$. However, only the stieltjesness of f was actually used there, and the main algorithm and results of [3] can be automatically extended for $f(\lambda)$ given by (2.4) and any Stieltjes function in general.

It can be shown that the convergence of Padé–Chebyshev approximations is *superexponential* and the error obeys [4]

$$\max_{\lambda \in [\lambda_1, \lambda_2]} |f(\lambda) - f_k(\lambda)| = O(e^{-c l_{\max} \log l_{\max}}) \tag{2.16}$$

with $c > 0$ depending on λ_1, λ_2. As here $[\lambda_1, \lambda_2] = [-\omega_{\max}^2, 0]$ and $\xi_i = -[\pi(i - 1/2)/L]^2$, it follows that the number n of resonances in (2.14) is given by the integer part of $(L\omega_{\max}/\pi) + 1/2$, which is approximately equal to twice the number of wavelengths corresponding to $\omega_{\max}$ within $[0, L]$. Thus we arrive at an important conclusion that the exponential superconvergence occurs after the average grid density exceeds two points per minimum wavelength, i.e., the Nyquist limit. So, similarly to spectral methods, our finite difference scheme asymptotically (for high frequencies) requires only two grid points per wave length to converge.

2.2. Optimal grid construction. Having obtained numbers y_i, θ_i for $i = 1, \ldots, k$, we now calculate the gridsteps $h_i, \hat{h}_i$. We assume the normalization $\sum_{i=1}^{k} s_i^2 = 1$ and compute $\hat{h}_1 = 1/\sum_{i=1}^{k} y_i$ and $s_i^2 = \hat{h}_1 y_i$. We now need to solve the inverse spectral problem, i.e., to reconstruct the matrix H from its eigenvalues and the first components of its eigenvectors. This calculation is performed using a k-step recursive Lanczos algorithm that is presented, e.g., in [5]. To avoid loss of orthogonality of the Lanczos vectors in finite precision arithmetic, we use reorthogonalization [5].

Once the matrix H is obtained and $\hat{h}_1$ is known, we can calculate $h_i, \hat{h}_i$ using (2.10):

Step 2. Calculate $h_1 = -(\hat{h}_1 \alpha_1)^{-1}$ and for $i = 2, \ldots, k$

$$\hat{h}_i = (\beta_{i-1} h_{i-1}^2 \hat{h}_{i-1})^{-1}, \qquad h_i = -(\alpha_i \hat{h}_i + 1/h_{i-1})^{-1}. \tag{2.17}$$

The well-posedness of the resulting finite-difference schemes (2.5)–(2.6) (which is equivalent to positiveness of $h_i, \hat{h}_i$) is discussed in [3].

We conclude this section by considering the two-point Neumann problem, i.e., by imposing the following boundary conditions on (2.2):

$$v(0) = -1/\sqrt{\lambda}, \qquad v(L) = 0. \tag{2.18}$$

The impedance is defined as

$$u(0) = f(\lambda) = \frac{1 + e^{-2L\sqrt{\lambda}}}{\sqrt{\lambda}(1 - e^{-2L\sqrt{\lambda}})} = \frac{2}{L}\sum_{i=1}^{\infty} \frac{1}{\lambda - \xi_i}, \tag{2.19}$$

where $\xi_i = -[\pi(i-1)/L]^2$. For finite-difference approximation of (2.2)–(2.18) we take the scheme (2.5) with $v_k = 0$, $u_k \neq 0$. The optimal grid is generated using the same algorithm with the new expression for resonances ξ_i.

2.3. Experiment 1—A one-dimensional problem. To illustrate the developed technique we consider a problem for (2.1) on $[0, 1] \times [0, 5]$ with the homogeneous initial conditions and boundary conditions $\hat{v}(0, t) = -\frac{\partial g(t)}{\partial t}$, $\hat{u}(1, t) = 0$. Here $g(t)$ is a wavelet which is close to the Gaussian pulse $e^{-27(t-0.225)^2}$. The exact solution of this problem is $\hat{u} = g(x - t) + \sum_{i=1}^{\infty} (-1)^i [g(x - t + i + 1) + g(x + t - i - 1)]$. The cutoff frequency for g is approximately 90, so we execute the grid generation algorithm with $\omega_{\max} = 90$ and with $k = 35$. The spectral distribution of the error (as a function of $\lambda = -\omega^2$) is presented in Fig. 1. As we see, the approximation error is very small within the targeted spectral interval $[-8100, 0]$. The grid is shown in Fig. 2; its main features are the staggeredness (potential and derivative points

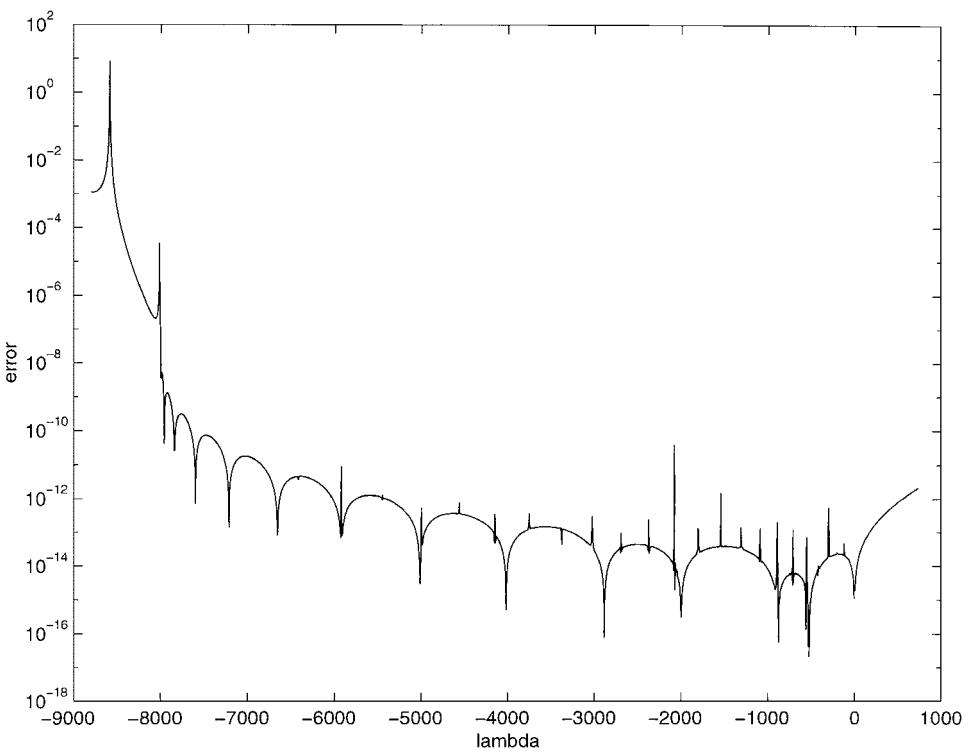

FIG. 1. The finite-difference impedance error.

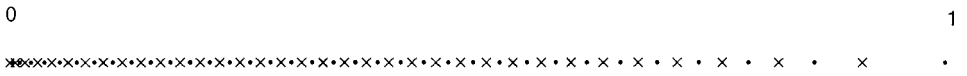

FIG. 2. Grid, $k = 35$; the $\cdot$ are x_k; the $\times$ are $\hat{x}_k$.

alternate), which was not imposed a priori on the grid generation algorithm, and gradual refinement toward $x = 0$, which is similar to one of the Legendre–Gauss–Lobatto points. The grid has about 2.5 grid points per minimal wavelength on average, but some steps are even larger than the wavelet size.

The finite-difference solution of this hyperbolic problem is obtained using the standard explicit FDTD with equal time steps. A two-dimensional plot of the finite-difference solution $\hat{u}$ is presented in Fig. 3. Due to the grid coarsening the wavelet becomes greatly distorted when it moves away from $x = 0$, but the distortion is almost completely reversed when the wave moves back after it hits the opposite boundary. Such behaviour is counterintuitive, because usually the finite-difference errors of hyperbolic equations propagate along characteristics. However, in our grid generation algorithm we approximately minimize the error of the finite-difference impedance at the targeted interface and spectral interval, and that is why we observe the local cancellation of the finite-difference dispersion error. We separately plotted the slices of the finite-difference solution at the targeted boundary and at the center of the interval in Fig. 4. Although the numerical dispersion at the target does not exceed 1% (the finite-difference solution almost exactly coincides with

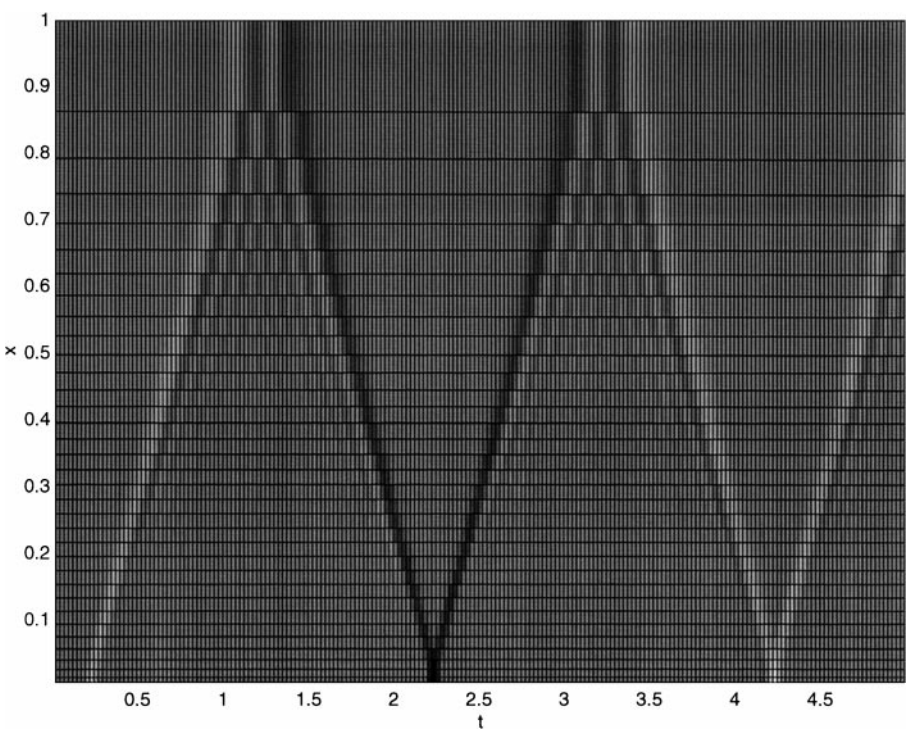

FIG. 3. The finite-difference solution on the optimal grid for Experiment 1, (t, x) coordinates. After every reflection the numerical dispersion is reversed.

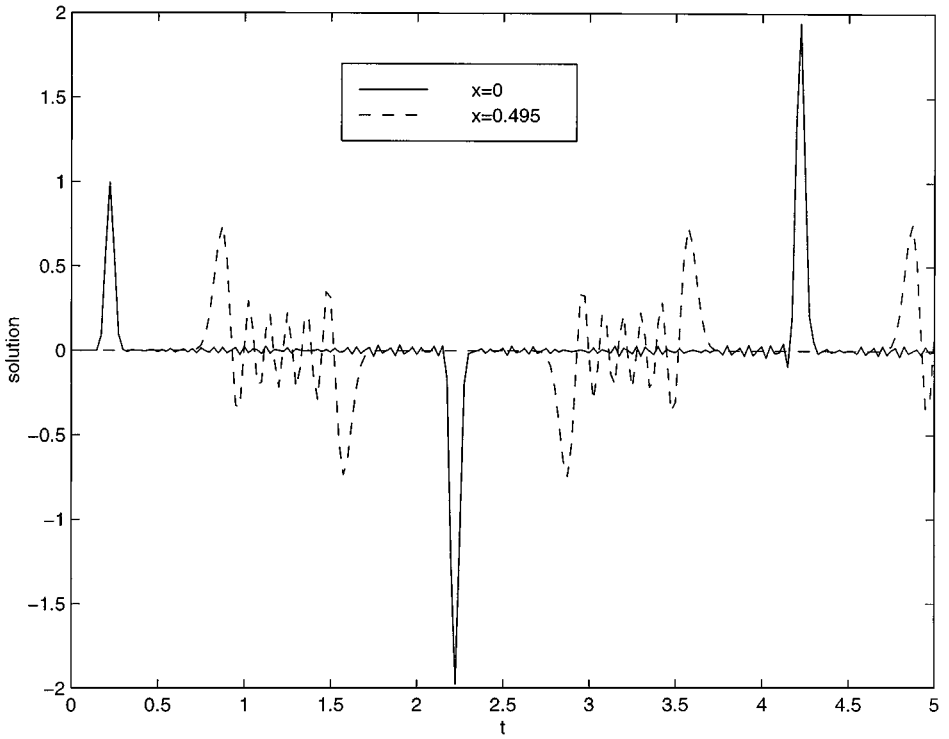

FIG. 4. The finite-difference solution at $x = 0$ and the center of the spacial interval.

the properly shifted and superposed wavelet), the error at the center of the spacial interval is larger then 50% of the signal and the shape of the wavelet is greatly distorted.

Finally, for comparison, we add to the optimal grid one potential and one derivative nodes at points $(x_{34} + x_{35})/2$ and $(\hat{x}_{34} + \hat{x}_{35})/2$, respectively. This change of the grid decreases the maximal grid step (and apparently the local finite-difference truncation error), so one would expect that it would decrease the numerical dispersion, but according to Fig. 5 the result is completely opposite. The point of this illustration is that the targeted error cancellation of the optimal grid can be destroyed even by unbalanced decrease of local truncation error.

3. ONE-DIMENSIONAL MULTIDOMAIN PROBLEMS FOR THE HELMHOLTZ EQUATION

To be able to consider hyperbolic problems with piecewise homogeneous media and to obtain exponential convergence at points that are interior to the computational domain, we first study the 1-D Helmholtz equation with piecewise constant coefficients. We start this section by looking at a two interval problem and derive a conjugation condition that will be extended to the case of several subdomains.

3.1. Two interval problem. Consider the Helmholtz equation on the interval $[-L_1, L_2]$ with a "potential" source defined at point $x = 0$:

$$m\lambda u - u_{xx} = \delta(x), \qquad u(-L_1) = u(L_2) = 0. \tag{3.1}$$

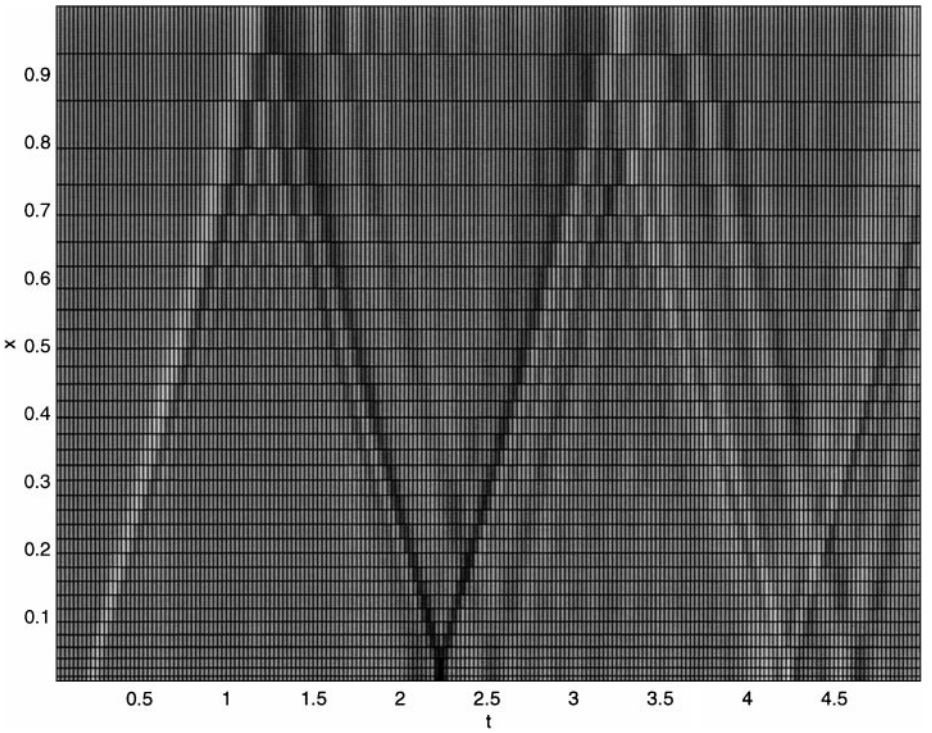

FIG. 5. The finite-difference solution in (t, x) coordinates, the optimal grid unbalanced by additional nodes. The numerical dispersion grows monotonically vs time.

This equation can be written as a first order system:

$$m\sqrt{\lambda}u = v_x + \delta(x)/\sqrt{\lambda}, \qquad \sqrt{\lambda}v = u_x, \qquad u(-L_1) = u(L_2) = 0. \tag{3.2}$$

We let the "media" be piecewise constant:

$$m = m(x) = \begin{cases} m_1, & x \in [-L_1, 0), \\ m_2, & x \in (0, L_2]. \end{cases} \tag{3.3}$$

This problem can be reduced to problem (2.2)–(2.3) on two subintervals. We note that $u(x)$ is continuous and that $v(x)$ satisfies

$$v(0+) - v(0-) = -1/\sqrt{\lambda}. \tag{3.4}$$

Let functions f_l, $l = 1, 2$, denote the impedance functions defined by (2.4) with $L = L_l$. Evidently,

$$u(0) = f_1(\lambda)v(0-)\sqrt{\lambda} = -f_2(\lambda)v(0+)\sqrt{\lambda}. \tag{3.5}$$

The difference in signs in the formula above results from the fact that to make the equations compatible with the previous formulation we let $x \to -x$ for the subinterval $[-L_1, 0]$. Let $h_{l,i}, \hat{h}_{l,i}$, $i = 1, \ldots, k$, $l = 1, 2$ be the steps obtained by the algorithm for (2.2)–(2.3) with

$L = L_l$, and let $f_{l,k}$ be the corresponding FD impedance functions. We approximate (3.2) by the following scheme. For $l = 1, 2$

$$\begin{aligned} m_l\sqrt{\lambda}u_{l,i} &= \eta_l \frac{v_{l,i} - v_{l,i-1}}{\hat{h}_{l,i}}, \qquad i = 1, \ldots, k, u_{l,k+1} = 0, \\ \sqrt{\lambda}v_{l,i} &= \eta_l \frac{u_{l,i+1} - u_{l,i}}{h_{l,i}}, \qquad i = 1, \ldots, k, \end{aligned} \tag{3.6}$$

together with the conjugation conditions

$$v_{2,0} - v_{1,0} = -1/\sqrt{\lambda}, \qquad u_{1,1} = u_{2,1}. \tag{3.7}$$

Here $\eta_2 = 1$ and $\eta_1 = -1$ due to the substitution $x \to -x$ on subinterval $[-L_1, 0]$.

We would like to avoid the extra conditions (3.7). For this purpose we put $u_1 = u_{1,1} = u_{2,1}$ and observe that

$$v_{1,0} = m_1\sqrt{\lambda}u_1\hat{h}_{1,1} + v_{1,1}, \qquad v_{2,0} = -m_2\sqrt{\lambda}u_1\hat{h}_{2,1} + v_{2,1}, \tag{3.8}$$

i.e.,

$$\tilde{m}\sqrt{\lambda}u_1 = \frac{v_{2,1} - v_{1,1}}{\hat{h}_{2,1} + \hat{h}_{1,1}} + \frac{1}{\sqrt{\lambda}(\hat{h}_{2,1} + \hat{h}_{1,1})} \tag{3.9}$$

with $\tilde{m} = (m_1\hat{h}_{1,1} + m_2\hat{h}_{2,1})/(\hat{h}_{2,1} + \hat{h}_{1,1})$. The conjugation condition (3.9) will be used on the interfaces between regions of piecewise constant media as well as on the interfaces with sources. Of course, the error at $x = 0$ (for a fixed λ, which is not a resonance for either the continuous or the discrete operator) obeys

$$|u_1 - u(0)| = O(|f_1 - f_{1,k}| + |f_2 - f_{2,k}|). \tag{3.10}$$

Thus, the approximation yields superexponential convergence at $x = 0$, and at all other points of the grid it behaves like a standard solution of a three point scheme with second order convergence with respect to the maximal grid step.

Suppose now we need to solve a similar problem with a "derivative" source,

$$m\lambda u - u_{xx} = \frac{d\delta(x)}{dx}, \qquad u(-L_1) = u(L_2) = 0, \tag{3.11}$$

which, when written as a first order system, becomes

$$m\sqrt{\lambda}u = v_x, \qquad \sqrt{\lambda}v = u_x + \delta(x), \qquad u(-L_1) = u(L_2) = 0. \tag{3.12}$$

For this system $v(x)$ remains continuous, while $u(x)$ obeys $u(0+) - u(0-) = -1$. Hence, (3.12) can be approximated by scheme (3.6) with the conjugation conditions

$$u_{2,1} - u_{1,1} = -1, \qquad v_{2,0} = v_{1,0}. \tag{3.13}$$

To exclude these conditions from the discretized equations, we put $u_1 \approx [u(0+) + u(0-)]/2$, i.e., $u_{2,1} = u_1 - 1/2$, $u_{1,1} = u_1 + 1/2$. From (3.6) we then have

$$\begin{aligned} \hat{h}_{1,1}m_1\sqrt{\lambda}u_1 &= -(v_{1,1} - v_{1,0}) - m_1\sqrt{\lambda}\hat{h}_{1,1}/2, \\ \hat{h}_{2,1}m_2\sqrt{\lambda}u_1 &= +(v_{2,1} - v_{2,0}) + m_2\sqrt{\lambda}\hat{h}_{2,1}/2, \end{aligned} \tag{3.14}$$

and, using condition (3.13),

$$\tilde{m}\sqrt{\lambda}u_1 = \frac{v_{2,1} - v_{1,1}}{\hat{h}_{2,1} + \hat{h}_{1,1}} + \frac{\sqrt{\lambda}}{2}\frac{m_2\hat{h}_{2,1} - m_1\hat{h}_{1,1}}{\hat{h}_{2,1} + \hat{h}_{1,1}}, \tag{3.15}$$

with $\tilde{m}$ defined as in the case of a potential source. However, since u_1 approximates the average value of the discontinuous function $u(x)$ at $x = 0$, the equations for $v_{l,1}$ need to be adjusted:

$$\sqrt{\lambda}v_{l,1} = \eta_l\frac{u_{l,2} - u_{l,1}}{h_{l,1}} = \eta_l\frac{u_{l,2} - u_1}{h_{l,1}} + \frac{1}{2}\frac{\eta_l}{h_{l,1}}. \tag{3.16}$$

3.2. Multidomain problem. If the domain of computation is divided into more than two subintervals, a straightforward application of the scheme discussed above will not work because the boundary conditions are defined only for two external subintervals, but not for internal ones. To have well defined boundary conditions for every subinterval, we use a decomposition of the solution into odd and even parts. For internal subintervals, the "boundary" condition will be defined at the midpoint (Dirichlet for the odd part and Neumann for the even), and the appropriate grid steps can be generated using the algorithms presented in Section 2.

Consider an interval $[X_0, X_\Lambda]$ decomposed into Λ regions with interfaces at points X_l, $l = 1, \ldots, \Lambda - 1$. Let the "media" $m(x)$ be piecewise constant with discontinuities at interfaces X_l: $m(x) = m_l$ on $[X_{l-1}, X_l]$, $l = 1, \ldots, \Lambda$. We allow up to $\Lambda - 1$ potential sources of weight d_l to be defined at internal interfaces $X_1, \ldots, X_{\Lambda-1}$ (the case of derivative and/or mixed sources is treated similarly), which leads to the problem

$$m\sqrt{\lambda}u = v_x + \frac{1}{\sqrt{\lambda}}\sum_{l=1}^{\Lambda-1} d_l\delta(x - X_l), \tag{3.17a}$$

$$\sqrt{\lambda}v = u_x, \qquad u(X_0) = u(X_\Lambda) = 0. \tag{3.17b}$$

Consider an internal subinterval $I_l = [X_{l-1}, X_l]$, $l = 2, \ldots, \Lambda - 1$. Let $2L_l$ be the length of I_l and $\tilde{X}_l$ be its midpoint. For $x \in [X_{l-1}, \tilde{X}_l]$ let

$$u^N(x) = u(x) + u[X_l - (x - X_{l-1})] \qquad \text{and} \qquad u^D(x) = u(x) - u[X_l - (x - X_{l-1})], \tag{3.18}$$

be the even and odd parts of the solution $u(x)$, respectively. Evidently,

$$\left.\frac{du^N}{dx}\right|_{\tilde{X}_l} = 0; \qquad u^D(\tilde{X}_l) = 0. \tag{3.19}$$

We will approximate the odd and even parts of the solution on the first half of each interval separately and then reconstruct the true solution by linear combination

$$\begin{aligned} u(x) &= u^N(x) + u^D(x), \qquad v(x) = v^D(x) + v^N(x) \qquad \text{on } x \in [X_{l-1}, \tilde{X}_l], \\ u(x) &= u^N(x) - u^D(x), \qquad v(x) = v^D(x) - v^N(x) \qquad \text{on } x \in [\tilde{X}_l, X_l]. \end{aligned}$$

Clearly, such decomposition is unnecessary on the two external subintervals, but for simplicity of notation we can put $u^N = v^N = 0$, $u = u^D$, $v = v^D$ there.

In the discretization of (3.17a)–(3.17b) that follows, the symbol $*$ replaces either symbol N or D and is used purely for notational convenience. The discretization is that for $l = 1, \ldots, \Lambda$

$$\begin{aligned} m_l\sqrt{\lambda}u^*_{l,i} &= \eta^*_l \frac{v^*_{l,i} - v^*_{l,i-1}}{\hat{h}^*_{l,i}}, \qquad i_* = 1, \ldots, k_l, \\ \sqrt{\lambda}v^*_{l,i} &= \eta^*_l \frac{u^*_{l,i+1} - u^*_{l,i}}{h^*_{l,i}}, \qquad i_D = 1, \ldots, k_l,\ i_N = 1, \ldots, k_l - 1 \\ u^D_{l,k_l+1} &= 0, \qquad v^N_{l,k_l} = 0, \qquad u^N_{l,k_l+1} = 0. \end{aligned} \tag{3.20}$$

Here $\eta^D_l = \eta^N_l = 1$ for $l = 2, \ldots, \Lambda - 1$, i.e., for all internal subintervals, and for the external ones $\eta^D_1 = -1$, $\eta^D_{\Lambda-1} = 1$, $\eta^N_1 = \eta^N_{\Lambda-1} = 0$.

The continuity conditions (for potential sources) become that for $l = 1, \ldots, \Lambda - 1$

$$\begin{aligned} \eta^N_{l+1}u^N_{l+1,1} + \eta^D_{l+1}u^D_{l+1,1} &= \eta^N_l u^N_{l,1} - \eta^D_l u^D_{l,1} \equiv u_{l,1}, \\ \left(\eta^D_{l+1}v^D_{l+1,0} + \eta^N_{l+1}v^N_{l+1,0}\right) - \left(\eta^D_l v^D_{l,0} - \eta^N_l v^N_{l,0}\right) &= -\frac{d_l}{\sqrt{\lambda}}. \end{aligned} \tag{3.21}$$

In order to be able to exclude variables $v^*_{l,0}$ as before, we require $\hat{h}^D_{l,1} = \hat{h}^N_{l,1} \equiv \hat{h}_{l,1}$, $l = 1, \ldots, \Lambda$; we then obtain the conjugation conditions

$$\sqrt{\lambda}\tilde{m}_l u_{l,1} = \frac{\left(v^D_{l+1,1} + v^N_{l+1,1}\right) - \left(v^D_{l,1} - v^N_{l,1}\right)}{\hat{h}_{l+1,1} + \hat{h}_{l,1}} + \frac{d_l}{\sqrt{\lambda}\left(\hat{h}_{l+1,1} + \hat{h}_{l,1}\right)}, \tag{3.22}$$

with the average $\tilde{m}_l = \left(m_{l+1}\hat{h}_{l+1,1} + m_l\hat{h}_{l,1}\right)/\left(\hat{h}_{l+1,1} + \hat{h}_{l,1}\right)$. The fact that $\hat{h}^D_1$ equals $\hat{h}^N_1$ has only a minor effect on the properties of the optimal grid (in particular, the convergence remains superexponential).

We note that scheme (3.20) can be transformed to the time domain if multiplication by $\sqrt{\lambda}$ is everywhere replaced by differentiation with respect to time and division by $\sqrt{\lambda}$ of the source function in (3.22)—by time integration. The time dependent scheme can be discretized, e.g., by forward time stepping with the approximations to the unknown functions $u = u(x, t)$ and $v = v(x, t)$ staggered in time.

4. APPLICATION TO THE HIGHER-DIMENSIONAL TIME DOMAIN WAVE PROBLEM

For the discretization of the two- or higher-dimensional wave equation with, e.g., potential sources

$$\begin{aligned} m(\mathbf{x})u_t(\mathbf{x}, t) &= \nabla \cdot \mathbf{v}(\mathbf{x}, t) + \sum_{l=1}^{\Lambda} g_l(t)\delta(\mathbf{x} - \mathbf{x}_l), \\ \mathbf{v}_t(\mathbf{x}, t) &= \nabla u(\mathbf{x}, t), \qquad \mathbf{x} \in \Omega; \\ u(\mathbf{x}, t) &\equiv 0 \qquad \text{on } \partial\Omega, \end{aligned} \tag{4.1}$$

one can extend the scheme described in the previous section, if the coefficient $m = m(\mathbf{x})$ is piecewise constant with discontinuities on the boundaries of rectangular blocks. In this

case, one can consider a direct product of grids which can be either optimal, or equidistant, and apply the decomposition into subintervals described in the previous section for the directions, in which the grid is chosen to be optimal.

We implemented two 2-D time domain finite difference schemes, one of which ("standard") is based on a direct product of equidistant grids, while the other ("optimal") is based on a product of an equidistant grid in the x-direction and an optimal grid in the y-direction. We here discuss the results of several experiments by comparing the accuracy and convergence properties of these two implementations.

4.1. Experiment 2—Uniform media. In this experiment we solve (4.1) with $\mathbf{x} = (x, y)$ and $m(\mathbf{x}) = \text{const.}$ for $\mathbf{x} \in \Omega = [0, 1]^2$. (For clarity we here use SI units, e.g., Ω has an area of one square meter.) The "speed" $c = m^{-1/2}$ is chosen to be 1000 m/s. The source x_1 is located at $(x, y) = (0.5, 0.25)$ and the solution is recorded at a series of 9 receivers positioned at $(x, y) = (0.1, 0.75), \ldots, (0.9, 0.75)$. The source signal function $g_1(t)$ is the first derivative of a Blackman-Harris window centered at 10 kHz, as seen in Fig. 6. The signals at the receivers can be calculated analytically and are shown in Fig. 8; these signals were also computed by finite difference schemes using both "standard" and "optimal" programs.

From the spectrum of the signal (Fig. 7), which we consider negligible below -50 dB, and the speed of the media, we see that the minimum wavelength is approximately 3 cm. The mesh in the x-direction, which is equidistant for both programs, is chosen to be the same and very fine, so that it does not affect the convergence properties of either scheme. The discretization step in the x-direction is chosen to produce about 40 points per minimal wavelength (ppw), which is generally considered sufficient for accurate discretization for equidistant grids.

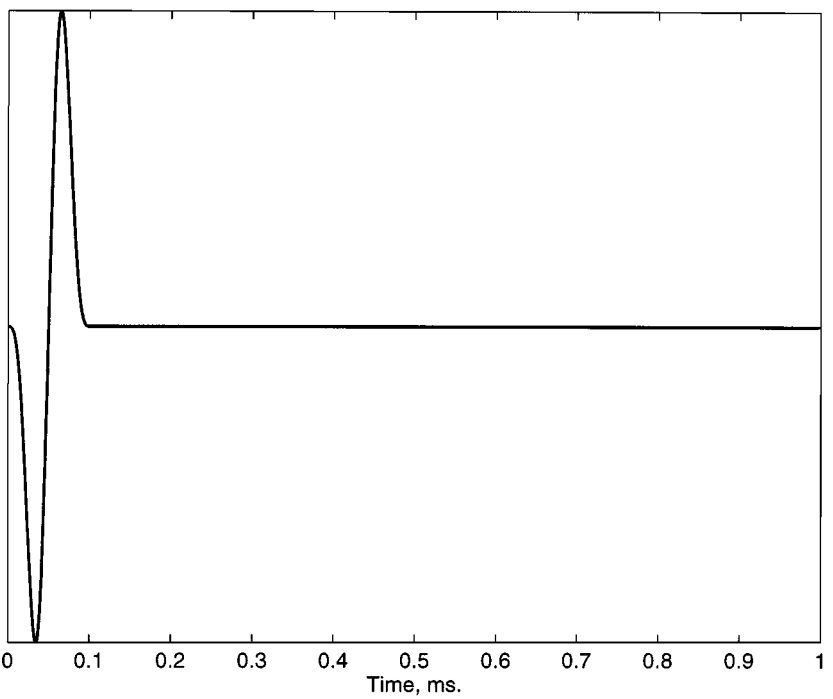

FIG. 6. Pulse function—first derivative of a Blackman–Harris window.

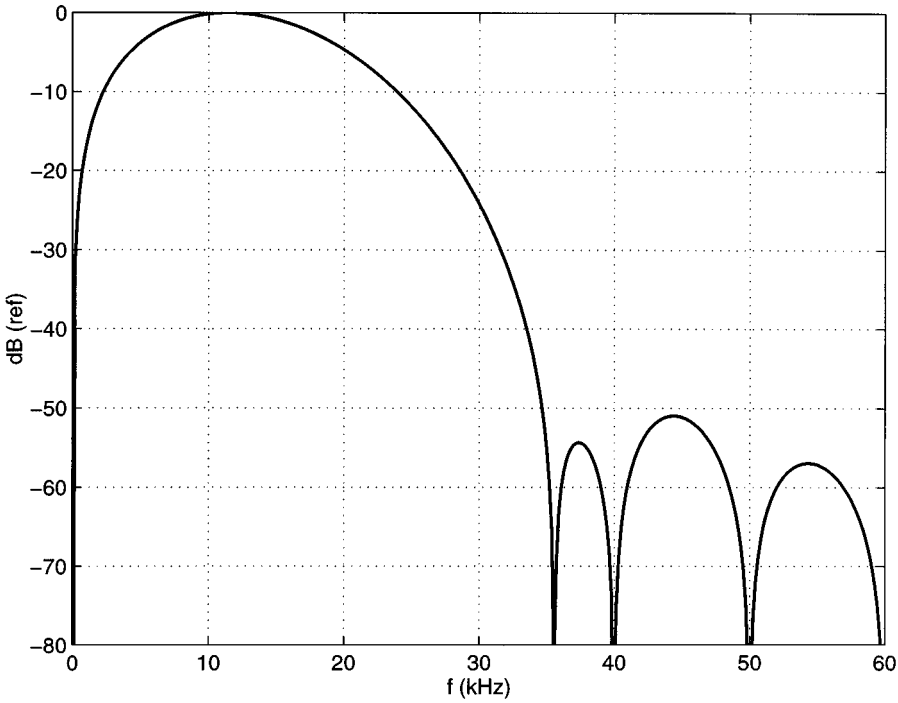

FIG. 7. The spectrum of the pulse function seen in the previous figure.

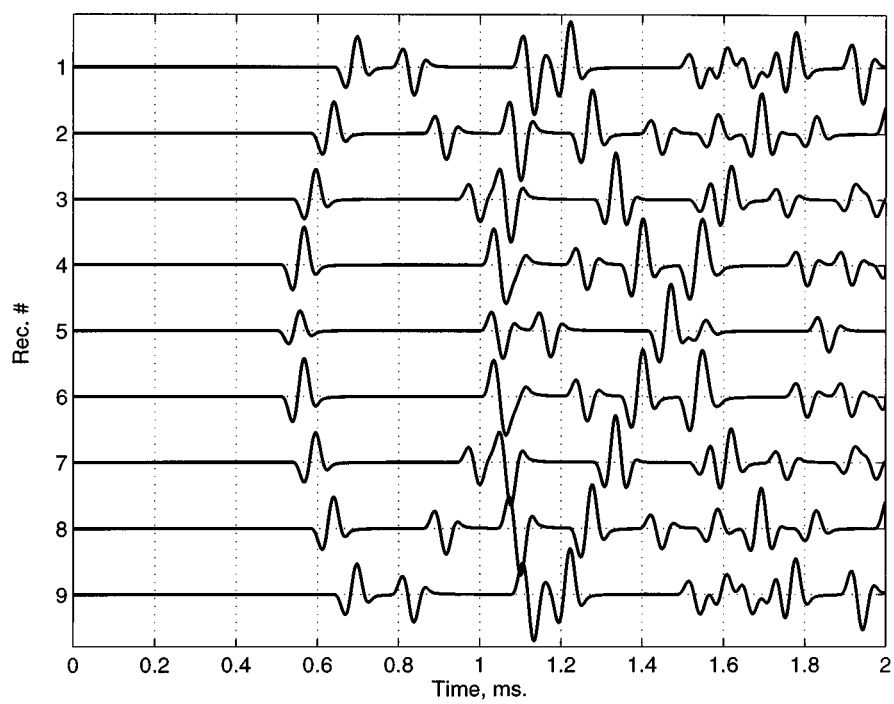

FIG. 8. Recorded signals for Experiment 2.

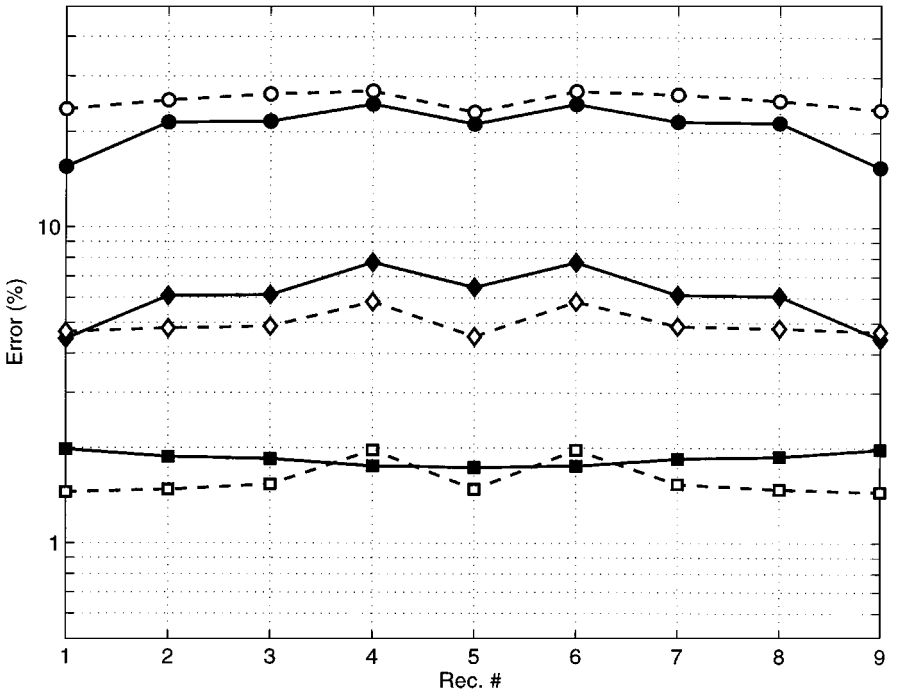

FIG. 9. L^2 error at receivers, Experiment 2. Dashed lines, "standard" program with 10, 20, and 30 ppw in Y; solid lines, "optimal" program with 1.7, 2.3, and 3.0 ppw in Y.

In Fig. 9 in dashed lines we show the discrepancies between the analytically calculated signals and those computed by the "standard" program with the y-direction discretization of 10, 20, and 30 ppw. We present the relative L^2 error on an interval $[0,\ T]$ with T being the maximum calculation time of 2 ms. The running times for these calculations are shown in Table I.

For the purposes of the "optimal" program, the domain Ω was decomposed in the y-direction into 3 regions: $I_1 = [0, 0.25]$, $I_2 = [0.25, 0.75]$, and $I_3 = [0.75, 1.0]$. The generation of the optimal mesh was performed according to Sections 1–3; the average density of gridpoints was chosen as 1.7, 2.3, and 3.0 ppw. The errors are presented in Fig. 9 by a solid line—one can see that for the desired accuracy of 1–2% the "optimal" program needs more than *10 times fewer* grid nodes than the "standard" one.

Because explicit time stepping was used in both programs, we need to consider the questions of stability of the time stepping operator. It turns out that the Courant condition is

TABLE I
Data for Experiment 2—Scalar Wave in Uniform Media

	Ppw in Y	Total pts in Y	Δt used (10^{-7} s)	Run time (s)
SP: run 1	10	360	6.9	1340
SP: run 2	20	700	6.3	2936
SP: run 3	30	1060	5.6	5247
OP: run 1	1.7	60	6.7	269
OP: run 2	2.3	80	6.1	401
OP: run 3	3.0	104	5.1	580

Note. SP, "standard" program; OP, "optimal" program.

slightly more restrictive for the "optimal" program, because, even though for it the *average* step size is larger than for the "standard" scheme, the stability condition is controlled by the minimum step size, which, for the "optimal" scheme, may be, and for the same accuracy is, slightly smaller. However, the running times presented in Table I show that even under the disadvantage of having a smaller time step, the "optimal" scheme performs much better in real time of calculation.

As expected, one sees from Table I that the running time for both the "standard" and the "optimal" programs is approximately proportional to the number of nodes in the y-direction divided by the time step used in the experiment. This confirms the claim that the optimal grid retains the same cost per grid node as the standard scheme. Thus, the overall advantage of using the "optimal" scheme is approximately one order of magnitude in real computational time or more if more accurate finite difference solutions are desired.

4.2. Experiment 3—Non-uniform media. In this experiment we considered a configuration consisting of rectangular blocks with three different speeds: the background media with $c_1 = 1000\sqrt{2}$ m/s, a fast horizontal layer with $c_2 = 1000\sqrt{3}$ m/s, and a slow vertical layer with $c_3 = 1000$ m/s on a rectangular domain $\Omega = [0, 1] \times [0, 2]$ m. The configuration is schematically presented in Fig. 10 and is chosen to remind a borehole intersecting a fast layer in a slow formation. A 10-kHz source is located at $(x, y) = (0.5, 0.25)$ and the signal is recorded at an array of 9 receivers which are positioned at equal intervals at $(x, y) = (0.1, 1.75), \ldots, (0.9, 1.75)$. We choose the source function and the slowest media the same as in Experiment 2; thus the minimal wavelength remains the same and we take the x-directional mesh (which is equidistant for both programs) to be the same as before, i.e., about 40 ppw.

The analytic solution to the above problem is not available; we therefore take as "true" the signals computed by the "optimal" program with 4 ppw in the y-direction (optimal mesh). Figure 11 presents the errors between the "true" signal and—in dashed lines—the signals computed by the "standard" program with 12, 30, and 50 ppw in the y-direction. By comparing Figs.11 and 9 we see that the accuracy of the "standard" scheme deteriorates when interfaces and angles are introduced into the problem. In fact, to obtain the goal accuracy of 1–2%, the density of gridpoints had to be increased from 30 to 40–50 points per wavelength.

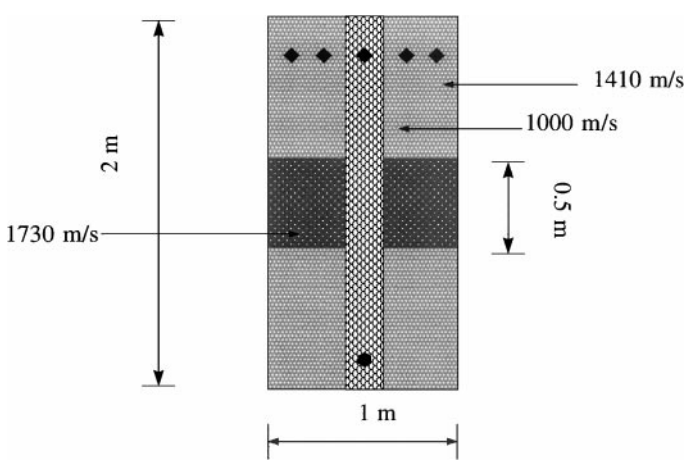

FIG. 10. Media for Experiment 3.

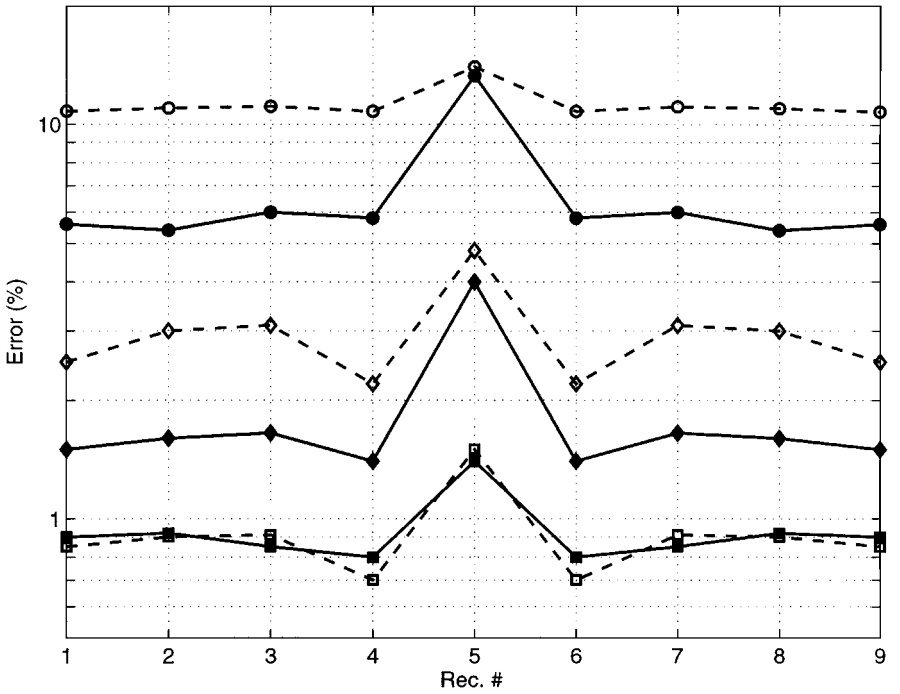

FIG. 11. L^2 error at receivers, Experiment 3. Dashed lines, "standard" program with 15, 30, and 50 ppw in y; solid lines, "optimal" program with 1.7, 2.3, and 3.0 ppw in y.

For the purposes of mesh generation for the "optimal" program, the domain Ω was decomposed into 5 subintervals in the y-direction, with interfaces at 0.25, 0.75, 1.25, and 1.75. The runs were made with 1.7, 2.3, and 3.0 ppw, and the errors are presented as solid lines in Fig. 11. We see that the quality of approximation of the "optimal" program is the same or even better than in the case of the uniform media. In fact, only the error of the signal at receiver 5, which is located in the slowest layer, is as large as in Experiment 2, while the errors at all other receivers are smaller. This is explained by the fact that the wave from the source to receiver 5 propagates mainly by the slower vertical medium, hence the average number of gridpoints per minimum wavelength is the smallest for that receiver, while for all other receivers the signal passes through faster medium and thus has longer wavelength (and more gridpoints per wavelength) on the average. In general, we observed that the approximation of the "optimal" program does not deteriorate with the introduction of interfaces and angles into the problem, and, in fact, the goal 1–2% accuracy was achieved at more than 15 times the speed of the "standard" program.

5. EXTENSION TO 2.5-D CYLINDRICAL ELASTICITY

We here consider equations of motion of a linear elastic isotropic body written in the form

$$\frac{d}{dt}\tau = \lambda(\nabla \cdot \mathbf{v})\mathbb{I} + \mu(\nabla\mathbf{v} + \nabla\mathbf{v}^T) + g\mathbb{I}, \tag{5.1}$$

$$\rho\frac{d}{dt}\mathbf{v} = \nabla \cdot \tau + \boldsymbol{f}, \tag{5.2}$$

where $\mathbf{v} = \mathbf{v}(\mathbf{x}, t)$ is the velocity vector, $\tau = \tau(\mathbf{x}, t)$ is the stress tensor, $\lambda = \lambda(\mathbf{x})$ and $\mu = \mu(\mathbf{x})$ are the Lame parameters, $\rho = \rho(\mathbf{x})$ is the density, $g = g(\mathbf{x}, t)$ is the pressure source, $\boldsymbol{f} = \boldsymbol{f}(\mathbf{x}, t)$ is the body force, and $\mathbb{I}$ is the identity tensor. When a cylindrical coordinate system is employed, Eqs. (5.1)–(5.2) can be written as

$$\frac{d}{dt}(MU) = DU + F, \tag{5.3}$$

where

$$U = \{v_r, v_\theta, v_z, \tau_{rr}, \tau_{\theta\theta}, \tau_{zz}, \tau_{r\theta}, \tau_{rz}, \tau_{r\theta}\}^T, \tag{5.4}$$

$M = M(\mathbf{x})$ is a symmetric, positive-definite matrix of material properties, D is, for appropriately chosen boundary conditions, a skew-symmetric differential operator, and F is the generalized source.

We implemented a finite difference discretization of system (5.3) in which the grid in the radial direction is kept equidistant and the axial direction grid is optimized. The optimization of the grid for the system of elasticity is performed using the algorithm described in Sections 1–3, with the usual staggering in space of elastic variables. We arbitrarily assign the nodes so that the diagonal component of the stress tensor is positioned in derivative points in both radial and axial directions.

The discretization scheme is designed so that, for equidistant grids and appropriate boundary conditions, it is energy preserving, in the sense that the finite difference operator (i.e., the discretization of operator D above) is skew-symmetric in the summation inner product. To simulate the response of an infinite medium, perfectly matched layer (PML) absorbing boundary conditions were used.

5.1. Experiment 4—A well in a layered media. We here take as an example a case of a borehole in a soft formation with a thin fast layer. The dipole ring pressure source is separated by 1 m from a vertical array of 4 receivers, which are located at 15 1-cm intervals. The source function is again the first derivative of the Blackman–Harris window, centered at 7.5 kHz. The parameters of the media are given in Table II.

We first note that if the layer is not present in the problem, even a coarse discretization in the radial direction gives a very good approximation of the correct solution (which in this case can be calculated by semi-analytic techniques, e.g., by real axis integration). In particular, we find that even a discretization with 10 points per wavelength in r (and an optimal grid in z of about 3 ppw) produces an error of less than a tenth of a percent.

When we introduce the fast 50-cm layer into the problem between the source and the first receiver, we no longer have the capability to calculate the correct signals by analytic techniques. We therefore take as the reference signals the ones calculated with 36 ppw in

TABLE II
Data for Experiment 4—Well in a Layered Media

Media	Density kg/m^3	Compressional speed m/s	Shear speed m/s
Background formation	2054	1890	508
Fast layer	2350	3658	2032
Water	1000	1500	0

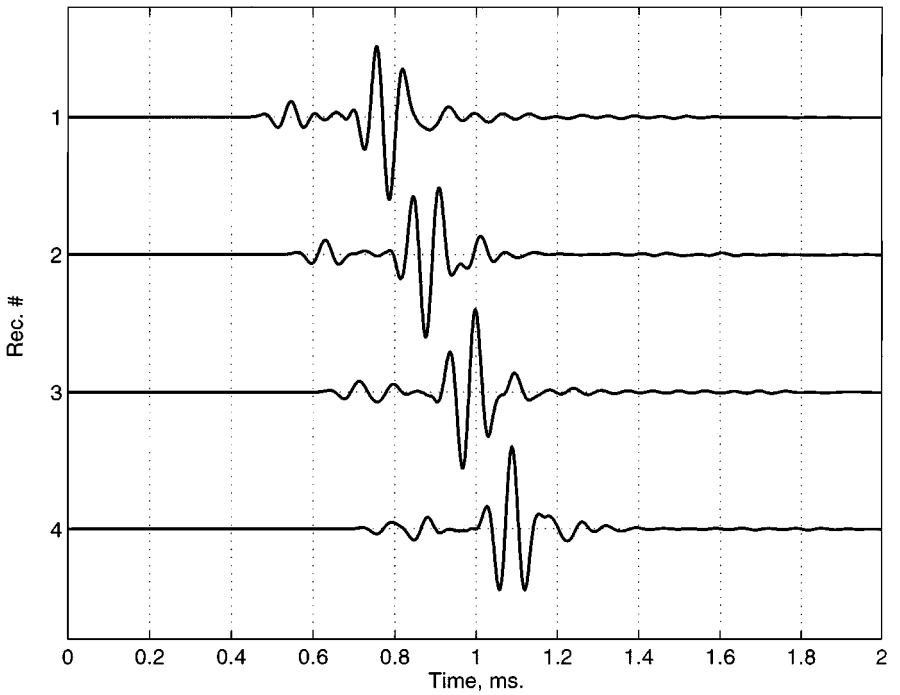

FIG. 12. Recorded signals, Experiment 4.

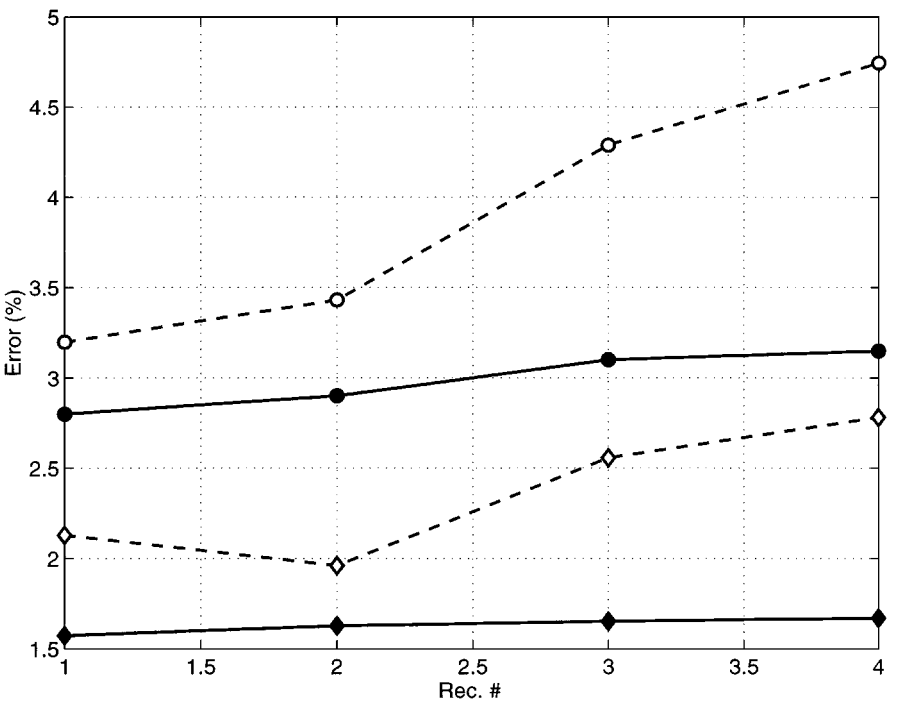

FIG. 13. L^2 error at receivers, Experiment 4. Dashed lines, "standard" program with 12 and 25 ppw in z; solid lines, "optimal" program with 2.5 and 3.0 ppw in z.

r-direction and the optimal mesh that theoretically produces 0.1% error in the z-direction (this mesh corresponds to an average of 3.25 ppw). It is interesting that the *minimum* step in the z optimal mesh that was chosen by the program is only about 10% bigger than the step in the r-direction. Figure 12 shows the resulting signals.

Figure 13 shows the change in the discrepancy between the reference and the calculated signals with the refinement of the optimal mesh in the axial direction and the refinement of the equidistant mesh in the radial direction. The r-directional (equidistant) mesh was fixed at 12 ppw for both programs. In dashed lines we show the errors in the signals computed in the two runs of the standard program, with 12 and 25 ppw in the z-direction. In solid lines we show the errors produced by the optimal program with 2.5 and 3.0 ppw. We here again see that for the goal accuracy of 1–2% the optimal program needs about 10 times fewer gridpoints in a given direction and thus performs approximately an order of magnitude faster in real computational time.

6. CONCLUSIONS

We have demonstrated that just a simple modification of the standard second order Cartesian finite-difference scheme (practically not affecting its computational cost) for hyperbolic elasticity problems exhibits at some a priori prescribed points the convergence properties of the spectral method: exponential convergence and good accuracy using only two to three grid points per wavelength.

The grid optimization performed along only one coordinate direction reduces the computational cost by approximately one order. We anticipate that the optimization with respect to both coordinates of the two-dimensional problem would speed up the solution by two orders and that, in principle, the acceleration of three-dimensional problems can be as large as three orders of magnitude.

The technique developed so far allows an obvious implementation only in the case of piecewise-homogeneous media with interfaces parallel to the Cartezian coordinate axes. Important topics of future research are extensions of the concept of optimal grids to non-rectangular domains, noncartesian coordinate systems, and problems with more general variations of coefficients. Another interesting future application of the Gaussian finite-difference rules can be the optimization of PML discretization.

REFERENCES

1. B. Fornberg, *Practical Guide to Pseudospectral Methods* (Cambridge Univ. Press, Cambridge, UK, 1996).
2. V. Druskin, *Spectrally Optimal Finite-Difference Grids in Unbounded Domains*, Schlumberger-Doll Research, Research Note, EMG-002-97-22, 1997.
3. V. Druskin and L. Knizhnerman, Gaussian spectral rules for the three-point second differences: I. A two-point positive definite problem in a semiinfinite domain, *SIAM J. Numer. Anal.*, accepted for publication.
4. V. Druskin and L. Knizhnerman, Gaussian spectral rules for the three-point second differences. II. Applications, *SIAM J. Numer. Anal.*, in press.
5. B. N. Parlett, *The Symmetric Eigenvalue Problem* (Prentice Hall/SIAM, Philadelphia, 1998).